Colloid and Polymer Science (2020) 298:663–679
https://doi.org/10.1007/s00396-019-04596-1

INVITED ARTICLE

Contrast variation of micelles composed of Ca^{2+} and block copolymers of two negatively charged polyelectrolytes

Nico Carl[1] · Sylvain Prévost[1] · Ralf Schweins[1] · Klaus Huber[2]

Received: 28 October 2019 / Revised: 19 December 2019 / Accepted: 19 December 2019 / Published online: 26 February 2020

Abstract

Block copolymers were prepared with two anionic polyelectrolyte blocks: sodium polyacrylate (PA) and sodium polystyrene sulfonate (PSS), in order to investigate their phase behavior in aqueous solution in the presence of Ca^{2+} cations. Depending on the concentration of polymer and Ca^{2+} and on the ratio of the block lengths in the copolymer, spherical micelles were observed. Micelle formation arises from the specific interaction of Ca^{2+} with the PA block only. An extensive small-angle scattering study was performed in order to unravel the structure and dimensions of the block copolymer micelles. Deuteration of the PA block enabled us to perform contrast variation experiments using small-angle neutron scattering at variable ratios of light and heavy water which were combined with information from small-angle X-ray scattering and dynamic light scattering.

Keywords Block copolyelectrolytes · Self-assembly · Specific interaction · Contrast variation · Micelles · Small-angle scattering

Introduction

Polyelectrolytes and their interactions with oppositely charged species such as ions, [1] surfactants [2–4], or charged surfaces [5] are essential to understand and control a variety of industrial processes. These include waste water treatment, [6] modification of the rheological behavior of concrete through superplasticizers [7, 8], or the properties of consumer goods such as shampoo [9]. The phase behavior of polyelectrolytes with several multivalent cations such as Ca^{2+}, [10, 11] Sr^{2+}, [11–14] Pb^{2+}, [15] Al^{3+} [16, 17], and La^{3+} [18, 19] has been extensively studied during the last decades. These aqueous systems show a rich phase behavior strongly depending on the polyelectrolyte, [20] cation, [16, 17, 21], temperature [16, 22], or concentration of inert salts such as NaCl [23].

Extensive work on the polyelectrolyte sodium polyacrylate (PA) addressed the specific interaction with Ca^{2+} [10, 11, 13, 23, 24]. Upon the addition of Ca^{2+}, the cation will bind to the negatively charged moieties of the PA chain. When the Ca^{2+} concentration is increased, more cations will bind to the polyelectrolyte until a critical concentration $[Ca^{2+}]_c$ is reached. Beyond this concentration, the polymer starts to aggregate and precipitate from the solution. A phase boundary according to

$$[Ca^{2+}]_c = r_0 + m[PA] \quad (1)$$

is found for this system where [PA] is the concentration of polyacrylate monomer units, r_0 the minimum concentration of Ca^{2+} required to precipitate the polymer at infinite dilution, and m defines the stoichiometry of binding. Precipitation at infinite dilution here means an intramolecular coil collapse. Equation 1 relates to a complexation equilibrium completely on the side of the Ca^{2+}/PA complex. Specificity of the interaction between Ca^{2+} and PA was further confirmed by isothermal titration calorimetry (ITC), which revealed a large endothermic heat. This large heat of reaction was interpreted by a liberation of around ten water molecules from hydration shells which coalesce upon complex bond formation between Ca^{2+} and two COO^- [25].

Electronic supplementary material The online version of this article (https://doi.org/10.1007/s00396-019-04596-1) contains supplementary material, which is available to authorized users.

✉ Klaus Huber
klaus.huber@upb.de

[1] Large Scale Structures Group, Institut Laue-Langevin, 71 Avenue des Martyrs, CS 20 156, 38042, Grenoble, France

[2] Chemistry Departement, University of Paderborn, Warburger Str. 100, 33098, Paderborn, Germany

Since one Ca^{2+} binds quantitatively to two polyacrylate monomer units, this system has for example been used for the design of an efficient Ca^{2+} sensor [26].

In contrast, another common polyelectrolyte polystyrene sulfonate (PSS) does not show specific interactions with Ca^{2+}. No matter how large the concentration of Ca^{2+} is set, no precipitation of the polymer does occur. Furthermore, light scattering demonstrated that the polymer chains do not even aggregate in the presence of Ca^{2+}. Isothermal titration calorimetry revealed just a weak endothermic signal, suggesting that the addition of Ca^{2+} induces only a replacement of two Na^{+} cations condensed into the polyelectrolyte domains by one Ca^{2+} and thus confirming the lack of any binding of Ca^{2+} to the sulfonic residues of PSS [20].

In a previous work, we combined these two different interaction patterns in one polymer by synthesizing a block copolymer (PA-*b*-PSS) of sodium polyacrylate and sodium polystyrene sulfonate [27]. Whereas the anionic residues of the PA block interact specifically with Ca^{2+}, no such interactions are expected for the PSS block. Indeed, it turned out that the block copolyelectrolytes form micelles in aqueous solution. Application of small-angle neutron scattering (SANS) at variable scattering contrasts, revealed the morphology of these micelles: The PA blocks change their solution behavior in water as specific interactions trigger decoration of PA with Ca^{2+} cations thereby establishing the core of the micelles. The PSS blocks keep their charges along the polymer backbone due to the lack of any specific interactions and form the stabilizing corona of the micelles. The entropic nature of the specific interactions between Ca^{2+} and PA enabled us to reversibly form and disintegrate the micelles by oscillating the temperature with an increase of temperature inducing formation and a decrease disintegration.

The present work extends the achievements published in Ref. [27] with the following new results: It interprets SANS and SAXS curves with a model [28] giving access to the morphology of the micellar corona, it outlines the benefit of combining SANS at variable contrast with SAXS, and it makes full use of Stuhrmann's approach [29, 30] in order to unravel the species in the core as well as the core dimensions independently of any model. All these features are established with three different block copolyelectrolytes: one sample with similar block lengths and the PA block fully deuterated and two samples with short PSS blocks and long PA blocks whereby in one case the PA block is fully deuterated and in the other case it is hydrogenated. This for the first time makes accessible a detailed comparative discussion.

The work is grouped in four parts: in the first part, we shortly revise the results on PA-*b*-PSS published in our preceding work, [27] in order to help the reader understanding the basis of the present work and to clearly separate it from the previous one. The second part deals with the comparative analysis of a contrast variation SANS experiment of three different block copolymers using a form factor model for micelles based on block copolymers [28]. The result is a comprehensive structural picture of the micelles. In particular, the advantage of joint SANS and SAXS experiments on the same set of samples is demonstrated and used to unravel an isotope effect occurring for two samples. The isotope effect results in a change of aggregation numbers, which was taken into account in the data analysis. The third part investigates the origin of this isotope effect using isothermal titration calorimetry and relates it to the binding of Ca^{2+} to PA. The fourth part demonstrates a model-independent analysis, which yields quantitative structural information. The obtained information is verified against the results from the form factor fits and can be used for systems where mathematical expressions for a form factor model are not available. It is demonstrated that this approach even works on a fully hydrogenated block copolymer, which has important implications for samples where deuteration is impractical or not feasible.

Experimental details

Materials

Light water (H_2O) was purified using a Milli-Q-system (Millipore) to a final resistivity of 18.2 MΩ cm. Heavy water (D_2O, Euriso-top, France, 99.90 atom% deuterium) was filtered with 100-nm PVDF filters (Merck Millex SLVV033RS) prior to use. $CaCl_2{\cdot}2H_2O$ (Sigma Aldrich, France, >99.9%), NaCl (Sigma Aldrich, France, >99.9%), and NaOH (Sigma Aldrich, France) were used as received.

Polymer synthesis and characterization

The synthesis and characterization of the polymers were described in detail in a previous work [27]. Figure 1 shows the chemical structure of the used polymers. All

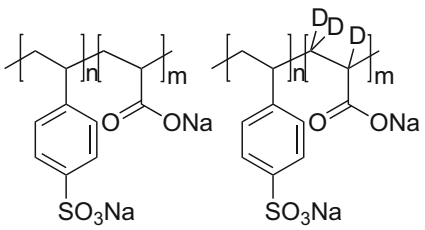

Fig. 1 Chemical structure of the used polymers. The left structure shows the fully hydrogenated polymer (h_3-PA-*b*-PSS). The right structure shows a polymer with a PA block which is fully deuterated (d_3-PA-*b*-PSS)

polymers were used as sodium salt. Prior to the small-angle scattering experiments the polymers and their phase behavior with Ca^{2+} were characterized using NMR and static and dynamic light scattering respectively. Detailed information can be found in the previous work [27]. Table 1 summarizes the results of the polymer characterization.

Sample preparation

The sample preparation was performed similarly as in previous works [22–24, 27]. The total number of positive charges for all samples was adjusted to 100 mmol L^{-1}. The total concentration of positive charges [+] is

$$[+] = [\mathrm{NaCl}] + 2 \cdot [\mathrm{CaCl_2}] = 100 \text{ mmol L}^{-1} \quad (2)$$

with [NaCl] being the concentration of sodium chloride and [$CaCl_2$] the concentration of calcium chloride. A sample containing 25 mmol L^{-1} $CaCl_2$ also contained 50 mmol L^{-1} NaCl, whereas a sample with 50 mmol L^{-1} $CaCl_2$ contains no additional NaCl.

SANS

SANS measurements were performed at the D11 small-angle scattering instrument of the Institut Laue-Langevin (Grenoble, France). Three sample to detector distances (39.0 m collimation 40.5 m, 8.0 m collimation 8.0 m, 1.4 m collimation 5.5 m) and a neutron wavelength of 0.5 nm (FWHM 9 %) were used to cover a q-range of $2{\cdot}10^{-2}\mathrm{nm}^{-1} - 5\ \mathrm{nm}^{-1}$. We used a circular neutron beam with a diameter of 15 mm. Scattered neutrons were detected with a ^{3}He MWPC detector (CERCA) with 256 × 256 pixels of 3.75 × 3.75-mm pixel size. Samples were filled in 2-mm Hellma 404 Quartz Suprasil cells. The sample temperature was adjusted to 25 °C using a circulating water bath. The detector images were azimuthally averaged, corrected to transmission of the direct beam, and scaled to absolute intensity using the LAMP software. Scaling to absolute intensity was based on a 1-mm H_2O cell as secondary calibration standard ($\frac{d\Sigma}{d\Omega} = 0.929\ \mathrm{cm}^{-1}$ at a neutron wavelength of 5 Å). The scattering from the solvent and the incoherent background were subtracted from the scattering curves. Details for the data reduction can be found in Chapter 2 of Ref. [31].

Table 1 Overview of polymers, compositions, weight-averaged molecular weights M_w, and hydrodynamic radii R_h determined from NMR and static and dynamic light scattering in 100 mmol L^{-1} NaCl as a good solvent and in the absence of $CaCl_2$

Sample	PA:PSS / mol%	M_w/ kg mol^{-1}	R_h/ nm
h_3-$PA_{1190}PSS_{70}$	94:6	160 ± 2	13.8 ± 0.6
d_3-$PA_{1190}PSS_{70}$	94:6	181 ± 3	13.6 ± 0.5
d_3-$PA_{360}PSS_{400}$	47:53	127 ± 1	10.4 ± 0.2

The subscript denotes the degree of polymerization, while d_3 and h_3 correspond to the deuteration or hydrogenation of the PA block, respectively

SAXS

Small-angle X-ray scattering was performed at the ID02 beamline of the European Synchrotron Radiation Facility (ESRF). Two sample to detector distances (10 m and 1 m) were measured at an X-ray energy of 12.46 keV (0.0995 nm) using a Rayonix MX-170HS CCD detector to cover a q-range of $8{\cdot}10^{-3}\mathrm{nm}^{-1} - 6\mathrm{nm}^{-1}$. Samples were filled in 2-mm quartz glass capillaries (WJM Glas Müller, Berlin, Germany). The detector images were corrected for dark and flat-field, azimuthally averaged, corrected to transmission of the direct beam, and scaled to absolute intensity using water as a secondary standard [32, 33]. The scattering from the solvent was subtracted from the scattering curves. Details can be found in Ref. [33]. Error bars were estimated as standard deviations from measurements of at least five different positions within the capillary.

Small-angle scattering data analysis

The form factor of spherical self-assembled block copolymers with excluded volume interaction of the polymer chains in the corona [28] was used to fit the SAXS and SANS data. The specific macroscopic scattering cross-section per unit solid angle $\frac{d\Sigma}{d\Omega}(q)$ of a solution of micelles can be written as [28]

$$\begin{aligned}\frac{d\Sigma}{d\Omega}(q) = N\Big[&N_{\mathrm{agg}}^2\beta_{\mathrm{core}}^2 A_{\mathrm{core}}^2(q) + N_{\mathrm{agg}}\beta_{\mathrm{corona}}^2 P'_{\mathrm{corona}}(q)\\ &+ 2N_{\mathrm{agg}}^2\beta_{\mathrm{core}}\beta_{\mathrm{corona}} A_{\mathrm{core}}(q) A_{\mathrm{corona}}(q)\\ &+ N_{\mathrm{agg}}\left(N_{\mathrm{agg}} - P'_{\mathrm{corona}}(0)\right)\beta_{\mathrm{corona}}^2 A_{\mathrm{corona}}^2(q)\Big] \quad (3)\end{aligned}$$

where N is the number density of micelles, N_{agg} the aggregation number of micelles, and β_{core} and β_{corona} are the total excess scattering length of the block forming the spherical core and the corona, respectively. They are defined as

$$\beta_{\mathrm{corona}} = V_{\mathrm{m,\,corona}}\mathrm{DP}_{\mathrm{corona}}\Delta\rho_{\mathrm{corona}} \quad (4)$$

and

$$\beta_{\mathrm{core}} = V_{\mathrm{m,\,core}}\mathrm{DP}_{\mathrm{core}}\Delta\rho_{\mathrm{core}} \quad (5)$$

with V_{m} being the molecular volume of the respective monomer unit, $\mathrm{DP}_{\mathrm{corona}}$ and $\mathrm{DP}_{\mathrm{core}}$ the degree of polymerization of the corona and core block, and $\Delta\rho$ the corresponding excess scattering length density.

Equation 3 consists of four different contributions: scattering from the spherical homogeneous core $A^2_{\text{core}}(q)$, scattering from the polymer chains in the corona $P'_{\text{corona}}(q)$, the term which takes into account the cross-term between core and corona $A_{\text{core}}(q) \cdot A_{\text{corona}}(q)$, and a term which takes into account interferences between chains in the corona $A^2_{\text{corona}}(q)$. $A_{\text{core}}(q)$ is the scattering amplitude of a homogeneous sphere [34] with radius R_{core}

$$A_{\text{core}}(q) = 3\frac{\sin(qR_{\text{core}}) - qR_{\text{core}}\cos(qR_{\text{core}})}{(qR_{\text{core}})^3} \tag{6}$$

$P'_{\text{corona}}(q)$ is the form factor of a chain in the corona. It contains the self-correlation of the chain $P_{\text{exv}}(q)$ as well as the interaction between the chains, which is expressed by the interaction parameter ν [28, 35]

$$P'_{\text{corona}}(q) = \frac{P_{\text{exv}}(q)}{1 + \nu P_{\text{exv}}(q)} \tag{7}$$

where $P_{\text{exv}}(q)$ is the form factor of a semi flexible self-avoiding chain. This form factor was first derived by Pedersen and Schurtenberger [36] and later corrected [37]. In experiments, ν typically adopts values between 0 and 8 and is related to the osmotic compressibility κ by [28, 35, 38]

$$\kappa = 1 + \nu \tag{8}$$

$A_{\text{corona}}(q)$ is given by

$$A_{\text{corona}}(q) = \frac{\int \rho_{\text{corona}}(r) r^2 \frac{\sin(qr)}{qr} dr}{\int \rho_{\text{corona}}(r) r^2 dr} \tag{9}$$

with $\rho_{\text{corona}}(r)$ as the scattering length density profile in the corona. $A_{\text{corona}}(q)$ is normalized so that $A_{\text{corona}}(0) = 1$. In this work, we use a Gaussian profile, which is defined as

$$\rho_{\text{corona}}(r) = \begin{cases} 0 & \text{for } r < R_{\text{core}} \\ 1 & \text{for } r = R_{\text{core}} \\ \exp\left(\frac{-(r-R_{\text{core}})^2}{2s^2}\right) & \text{for } r > R_{\text{core}} \end{cases} \tag{10}$$

with s controlling the thickness of the corona.

In order to take into account the size distribution of micelles, we assumed a log-normal distribution of the aggregation number N_{agg}

$$p\left(N_{\text{agg}}\right) = \frac{1}{H\sqrt{2\pi}N_{\text{agg}}} \exp\left(\frac{-\log\left(N_{\text{agg}} - M\right)^2}{2H^2}\right) \tag{11}$$

where H and M define the distribution and are connected to the mean aggregation number $\overline{N_{\text{agg}}}$ and standard deviation $\sigma_{\overline{N_{\text{agg}}}}$ by

$$\overline{N_{\text{agg}}} = \exp\left(M + \frac{H^2}{2}\right) \tag{12}$$

$$\sigma_{\overline{N_{\text{agg}}}} = \sqrt{\exp\left(H^2 + 2M\right)\left(\exp\left(H^2\right) - 1\right)} \tag{13}$$

The macroscopic scattering cross-section is therefore

$$\frac{d\Sigma}{d\Omega}_{\text{polydisperse}}(q) = \int \frac{d\Sigma}{d\Omega}(q) p(N_{\text{agg}}) dN_{\text{agg}} \tag{14}$$

Instrumental resolution for SANS has been taken into account according to Ref. [39]. The macroscopic scattering function is convoluted with a resolution function $R\left(q, \sigma_q\right)$, which depends on wavelength spread, finite collimation of the beam, and detector resolution

$$\frac{d\Sigma}{d\Omega}_{\text{smeared}}(q) = \int R(q, \sigma_q) \frac{d\Sigma}{d\Omega}_{\text{polydisperse}}(q) dq \tag{15}$$

For the form factor fits, we used the SASET program [40], which allows global fitting of several contrasts at the same time. During the data analysis of the SANS curves, we took into account the instrumental resolution for each detector configuration and merged the data only for final representation. This approach allowed us to increase the number of available data points since we do not truncate the data in the region of overlapping q. The factor for merging the SANS measurements at 39 m to the other configurations was set as a global fitting parameter for all the curves as using water as an absolute calibration standard is not feasible at this sample to detector distance.

Dynamic light scattering

Dynamic light scattering (DLS) available in the ILL PSCM lab was performed using an ALV CGS-3 (ALV, Langen, Germany) equipped with a HeNe laser operating at $\lambda_0 = 632.8$ nm. The samples were filtered in cylindrical quartz glass cells using Millex PVDF filters with a pore size of 0.45 μm. The temperature of the samples was kept at 25 °C. DLS was measured in an angular range from 30° to 150° in steps of 10°.

The intensity-time correlation function $g_2(\tau) - 1$ was analyzed using the method of cumulants [41]

$$g_2(\tau) - 1 = B + \beta \exp(-2\Gamma\tau)\left(1 + \frac{\mu_2}{2!}\tau^2\right)^2 \tag{16}$$

B is a factor correcting the baseline, β a factor which depends on the experimental setup, and Γ the relaxation rate and μ_2 the second cumulant. The apparent diffusion coefficient $D_{app}(c, q)$ for a given q is calculated according to

$$D_{app} = \frac{\Gamma}{q^2} \tag{17}$$

The diffusion coefficient is extrapolated towards $q = 0$ according to [42, 43]

$$D_{app}(q) = D_0\left(1 + CR_g^2 q^2\right) \tag{18}$$

where C is a constant describing the q dependence of $D_{app}(q)$. The diffusion coefficient D_0 is used to calculate

the hydrodynamic radius R_h using the Stokes-Einstein equation

$$R_h = \frac{k_B T}{6\pi\eta D_0} \tag{19}$$

where T is the temperature, k_B the Boltzmann constant, and η the viscosity of the solvent.

The viscosity of D_2O and H_2O was obtained from Ref. [44], while for mixtures of D_2O and H_2O the viscosity was calculated based on the volume fraction.

Isothermal titration calorimetry (ITC)

Isothermal titration calorimetry (ITC) was performed using a VP-ITC calorimeter from Malvern Instruments at 25.0 °C. The cell contained 1.4 mL of a solution of PA (0.2 gL^{-1} in 100 mmol L^{-1} NaCl). To this solution, between 4 and 24 μL of an aqueous solution containing 12 mmol L^{-1} $CaCl_2$ and 76 mmol L^{-1} NaCl was added. The time span between the injections was 300 s. The experiment was repeated twice, first using H_2O as a solvent and then D_2O. The baseline correction and integration of the peaks was performed using the software NITPIC [45]. The signals were not corrected for the heat of dilution of the polyelectrolyte and the $CaCl_2$ solution as these contributions were considerably smaller than the heat of binding of Ca^{2+} to PA. The data were fitted using the model of a single set of identical binding sites [46, 47].

Results and discussion

Review of micellization of PA-*b*-PSS in the presence of Ca^{2+} [27]

Four polymers at three different ratios of block lengths were synthesized and investigated in the context of the previous work: two polymers with a long PA and a short PSS block (d_3-$PA_{1190}PSS_{70}$ and h_3-$PA_{1190}PSS_{70}$), one polymer with a symmetric block ratio between PA and PSS (d_3-$PA_{360}PSS_{400}$), and one polymer with a long PSS and a short PA block (h_3-$PA_{100}PSS_{750}$). In the presence of Ca^{2+}, d_3-$PA_{1190}PSS_{70}$ and d_3-$PA_{360}PSS_{400}$ form spherical block copolymer micelles arising from the specific interaction of Ca^{2+} with the PA block. In contrast, micelle formation was not observed for h_3-$PA_{100}PSS_{750}$ due to the considerably shorter PA block, not rendering the polymer chain hydrophobic enough to form micellar aggregates. Phase diagrams of the two polymers forming micelles were established and are presented in Fig. 2.

Contrast variation small-angle neutron scattering of the micelles was performed at variable H_2O/D_2O ratios using the two block copolymers with the deuterated PA

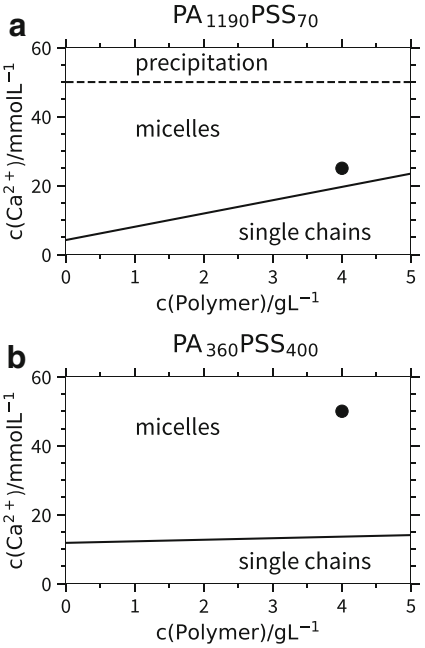

Fig. 2 Phase diagrams of **a** d_3-$PA_{1190}PSS_{70}$/h_3-$PA_{1190}PSS_{70}$ and **b** d_3-$PA_{360}PSS_{400}$ in the presence of Ca^{2+} at 25 °C. The black points indicate the states where the contrast variation experiments were performed

block, labelled as d_3-PA. The black dots in Fig. 2 indicate the sample composition where the contrast variation experiments were conducted. A preliminary analysis of the scattering data revealed that d_3-PA blocks complexed by Ca^{2+} form the hydrophobic core of the micelles, while PSS is located in the corona and stabilizes the aggregates.

Furthermore, it was shown that an increase of temperature promotes the binding of Ca^{2+} to PA and was therefore used to induce micelle formation of a sample close to the phase transition. It was demonstrated that micelle formation is reversible and can be induced and reverted by consecutive additions of Ca^{2+} and a complexing agent such as Na_2EDTA and by consecutive cycles of temperature increase and drop respectively.

Scattering analysis with a form factor model

The main motivation for performing a contrast variation experiment on the presented system is to figure out whether PSS or PA forms the hydrophobic core of the anticipated micellar aggregates. This was already elucidated in the previous work [27]; however, fitting the data with a form factor model also makes accessible information about the exact size of the micelle core, the water content inside the micelle core, and the thickness of the corona as well as the interaction of the polymer chains in the corona. In order to

assess such information, the model of a block copolymer micelle with self-avoiding chains in the corona (Eq. 3) was used to fit the experimental data [28]. In addition to the polymers d_3-$PA_{360}PSS_{400}$ and d_3-$PA_{1190}PSS_{70}$, a third fully hydrogenated polymer h_3-$PA_{1190}PSS_{70}$ is investigated in the current work. Deuteration is not always feasible as deuterated monomers do not exist for a wide range of polymers and deuteration of biological molecules such as proteins or sugars is often difficult and very cost intensive. Nevertheless, a contrast variation experiment is still possible if the scattering length densities of two components are sufficiently different. h_3-$PA_{1190}PSS_{70}$ will be used as a showcase to illustrate the feasibility of performing a contrast variation study on a fully hydrogenated block copolymer. The present section will present a comparative and exhaustive interpretation of the SANS and SAXS curves of all three block copolyelectrolyte samples with suitable model form factors [28].

Figure 3 shows the SANS profiles of d_3-$PA_{360}PSS_{400}$ micelles at variable H_2O/D_2O ratios. As has been outlined in Ref. [27], the overall shape and the forward scattering of the SANS profiles presented in Fig. 3 drastically change upon variation of the solvent ratio H_2O/D_2O. SAXS on the same samples was also performed to show that changing from light to heavy water does not influence the aggregation number, size, and morphology of the aggregates. Figure 4 a shows these SAXS profiles. All SAXS curves overlap perfectly (Fig. 4b), when plotted without the multiplication factor used in Fig. 4a. The perfect overlay of the SAXS curves clearly demonstrates that the variation in the D_2O/H_2O ratio does not affect the nature of the aggregates. This finding simplifies the interpretation of the scattering data from d_3-$PA_{360}PSS_{400}$ considerably.

Figures 5 and 7 show the SANS profiles of d_3-$PA_{1190}PSS_{70}$ and h_3-$PA_{1190}PSS_{70}$ micelles in six different H_2O/D_2O mixtures, and Figs. 6a and 8a show the SAXS profiles of the corresponding solutions. As observed for d_3-$PA_{360}PSS_{400}$, the forward scattering of the SANS curves changes with varying D_2O content. For d_3-$PA_{1190}PSS_{70}$, the forward scattering continuously decreases with increasing content of D_2O, while for h_3-$PA_{1190}PSS_{70}$ the forward scattering decreases until 54.0% D_2O and subsequently increases again.

Moreover, the slope at high q changes. This becomes particularly evident for the partly deuterated polymer when comparing Fig. 5c and f. In Fig. 5c, the PSS block is matched and a slope of -4 is found. The contrast in Fig. 5f is the closest possible one to the match of d_3-PA and shows a less step slope, which is closer to -2. The data at high q for the fully hydrogenated polymer show a higher statistical error than the data from the two other polymers. This can be attributed to the higher ^1H content of the fully hydrogenated polymer. Hence, the subtraction of the higher incoherent background introduces more noise to the data. This makes the determination of slopes at high q for this polymer difficult.

The SAXS profiles of d_3-$PA_{1190}PSS_{70}$ and h_3-$PA_{1190}PSS_{70}$ in Figs. 6a and 8a show well-defined form factor oscillations; however, a closer look at the position of the first minimum of $P(q)$ shows that q_{min} shifts to slightly higher values when the D_2O content is increased. This corresponds to a slightly changing micelle size when

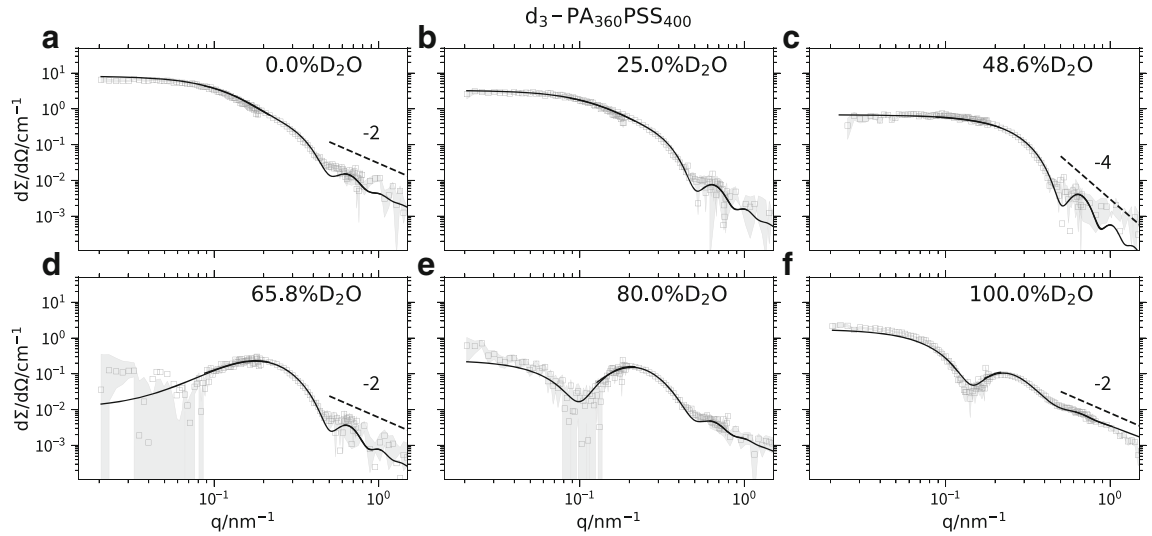

Fig. 3 SANS profiles of d_3-$PA_{360}PSS_{400}$ (c_{poly} = 4gL^{-1}, $c_{Ca^{2+}}$ = 50 mmol L^{-1}) in 0.0% D_2O (**a**), 25.0% D_2O (**b**), 48.6% D_2O (**c**), 65.8% D_2O (**d**), 80.0% D_2O (**e**), and 100.0% D_2O (**f**). The solid lines represent fits to the form factor of a polydisperse block copolymer micelle [28]. An overview of the fit results can be found in Table 2 and Table S3 of the Supporting Information

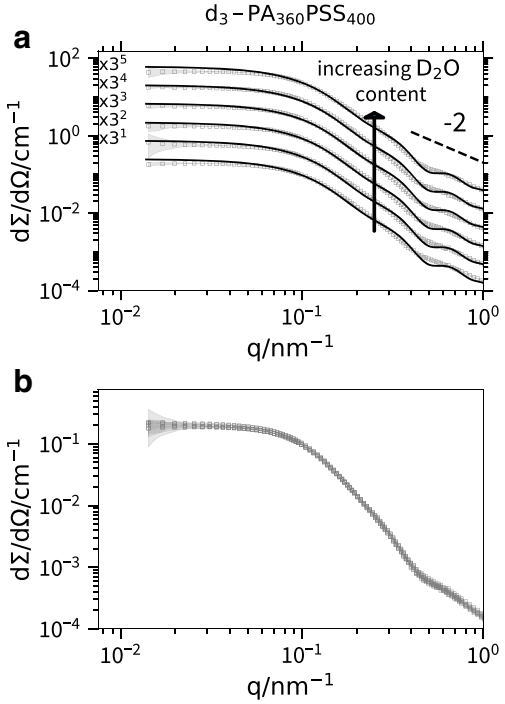

Fig. 4 SAXS profiles of d_3-$PA_{360}PSS_{400}$ (c_{poly} = 4gL^{-1}, $c_{Ca^{2+}}$ = 50 mmol L^{-1}) in 0.0% D_2O, 25.0% D_2O, 48.6% D_2O, 65.8% D_2O, 80.0% D_2O, and 100.0% D_2O. **a** The curves multiplied with an offset. **b** The curves without the multiplication factor. The solid lines represent fits to the form factor of a polydisperse block copolymer micelle [28]. An overview of the fit results can be found in Table 2 and Table S3 of the Supporting Information

changing the D_2O/H_2O ratio. As this feature is very hard to be identified with SANS curves only, it highlights the relevance of a combined SANS and SAXS experiment for all samples of a contrast variation study.

The scattering curves of all three samples were analyzed with two possible configurations: $Ca_{0.5}$-d_3-PA forming the core and PSS the corona as well as $Ca_{0.5}$-PSS forming the core and PA the corona. SANS profiles at different contrasts as well as the SAXS profiles of the same samples were analyzed simultaneously in a global fit. Furthermore, the fit was heavily constrained due to the knowledge of the polymer composition, polymer concentration, molecular volumes [48], and scattering length densities of the blocks and the solvent.

A structure factor was not considered during the data analysis since the data did not show any evidence for the presence of particle interaction such as an up- or downturn at low q. This is rather unusual for highly charged systems since these systems usually show long range interactions or aggregation [49].

However, for the present case, the absence of a structure factor contribution can be explained by the high ionic strength of the respective polymer solution, which was introduced by adding a certain amount of NaCl as "inert salt" (see Sample preparation for details). This addition of NaCl leads to a strong screening of the charges of the polyelectrolyte. We estimated the ionic strength and Debye length of the solution by assuming that every PA monomer unit binds 0.5 Ca^{2+} cations. For d_3-$PA_{360}PSS_{400}$, we obtain an ionic strength of 141 mmol L^{-1} and a Debye length of 0.81 nm and for d_3-$PA_{1190}PSS_{70}$/h_3-$PA_{1190}PSS_{70}$ an ionic strength of 98 mmol L^{-1} and a Debye length of 0.97 nm. Previous works [12–16] showed that this approach can be used to investigate the single chain behavior of homopolyelectrolytes as the added "inert salt" effectively screens interactions between the chains. In the case of the present work, this approach was used analogously and explains the lack of any significant impact of inter-micelle repulsions on the present scattering data.

The strong screening also results in a conformation of the PSS chains in the corona, which can be well described by a self-avoiding polymer. In previous works, the use of "inert salt" such as NaCl allowed to study the single chain behavior of homopolyelectrolytes such as PA and PSS [16, 23].

The best fit obtained from analyzing the data of d_3-$PA_{360}PSS_{400}$ with $Ca_{0.5}$-PSS forming the core and PA the corona is shown in Figure S4 of the Supporting Information. It poorly describes the features of the scattering curves. In contrast, the solid lines in Figs. 3 and 4a show the fits for d_3-$PA_{360}PSS_{400}$ with $Ca_{0.5}$-d_3PA forming the core. The main features of the experimental data are considerably better described by the model with a core consisting of d_3-PA [27, 28]. This nicely agrees with the conclusions drawn from our previous work [27], confirming once again the fact that d_3-PA/Ca^{2+} forms the core of the micellar aggregates, while PSS is located in the corona. The form factor model with PA/Ca^{2+} in the core was also used for the analysis of d_3-$PA_{1190}PSS_{70}$ and h_3-$PA_{1190}PSS_{70}$. The solid lines in Figs. 5, 6a, 7, and 8a show the form factor fits to the SANS and SAXS profiles. The model describes the data well for all contrasts. Unlike to the form factor analysis of the data from d_3-$PA_{360}PSS_{400}$, where the aggregation number turned out to be independent of the ratio H_2O/D_2O, the slightly changing micelle size with increasing D_2O content observed in the case of the two samples with the long PA block is taken into account by assuming individual aggregation numbers for each contrast. Therefore, each SANS and SAXS profile for a given contrast is attributed to an individual N_{agg}. All the other

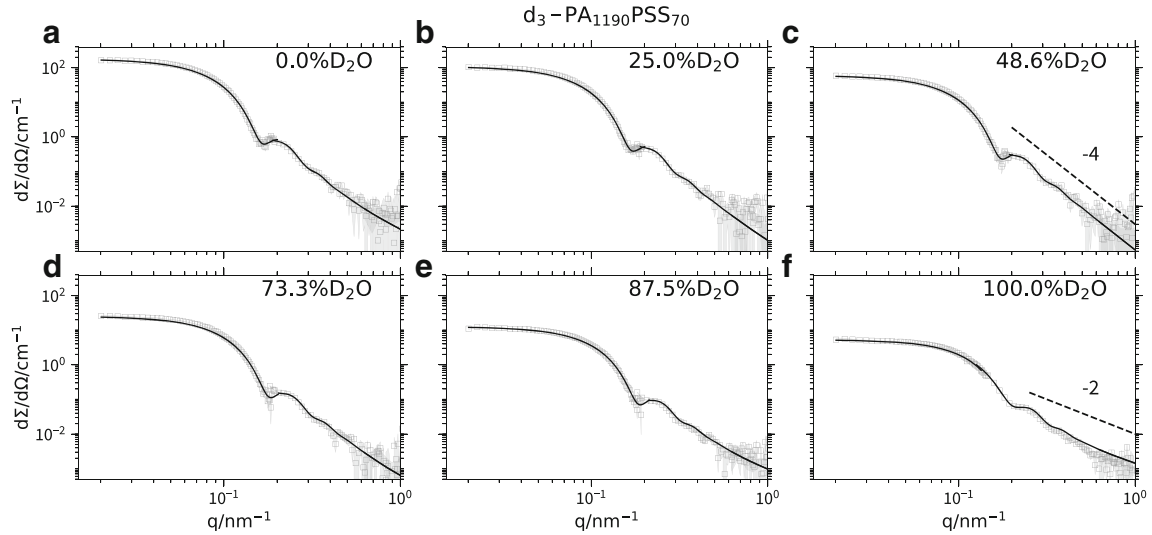

Fig. 5 SANS profiles of d_3-$PA_{1190}PSS_{70}$ (c_{poly} = 4gL^{-1}, $c_{Ca^{2+}}$ = 25 mmol L^{-1}) in 0.0% D_2O (**a**), 25.0% D_2O (**b**), 48.6% D_2O (**c**), 73.3% D_2O (**d**), 87.5% D_2O (**e**), and 100.0% D_2O (**f**). The solid lines represent fits to the form factor of a polydisperse block copolymer micelle [28]. An overview of the fit results can be found in Table 2 and Table S3 of the Supporting Information

fit parameters ($\frac{\sigma N_{agg}}{N_{agg}}$, $R_{g,corona}$, s, ν, h, $V_{m,\,Ca^{2+}}$) are fitted simultaneously for the whole data set. Table 2 summarizes the resulting fit parameters. The given aggregation numbers and core sizes for d_3-$PA_{1190}PSS_{70}$ and h_3-$PA_{1190}PSS_{70}$ are shown representatively for the sample in 100 % D_2O. Table S3 in the Supporting Information summarizes the aggregation numbers N_{agg} for the other contrasts.

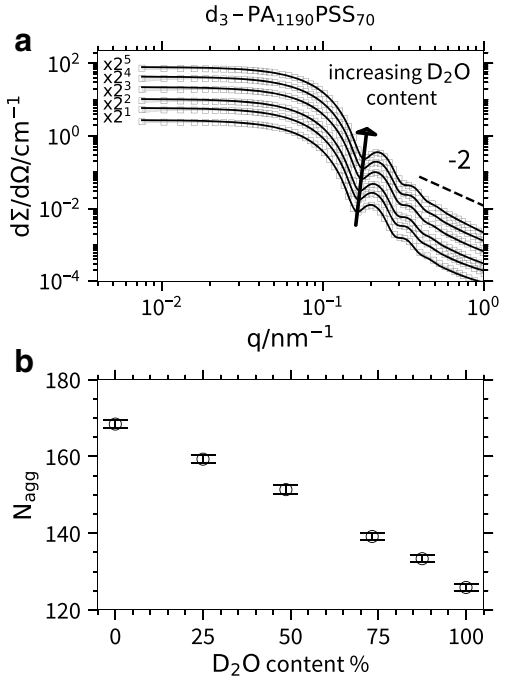

Fig. 6 **a** SAXS profiles of d_3-$PA_{1190}PSS_{70}$ micelles (c_{poly} = 4gL^{-1}, $c_{Ca^{2+}}$ = 25 mmol L^{-1}) in 0.0%, 25.0%, 48.6% , 73.3%, 87.5%, and 100.0% D_2O. The solid lines represent fits to the form factor of a polydisperse block copolymer micelle [28]. An overview of the fit results can be found in Table 2 and Table S3 of the Supporting Information. **b** Aggregation number of the micelles as a function of D_2O content

d_3-$PA_{360}PSS_{400}$ micelles have an aggregation number of 19 polymers per micelle. Compared to this the aggregation numbers of 168 $\geq N_{agg} \geq$ 126 for d_3-$PA_{1190}PSS_{70}$ and 145 $\geq N_{agg} \geq$ 117 for h_3-$PA_{1190}PSS_{70}$ are considerably bigger. This increase in aggregation number can be nicely reconciled with the increase of the PA block length as the block responsible for the formation of the poorly soluble core.

During the data analysis, it turned out that it is necessary to take into account a considerable amount of water in the core. Assuming a dry core consisting of polymer does not fit the data on absolute scale since aggregation number N_{agg} and number density of micelles N are strictly linked to the known polymer concentration. This heavily constrains the fit and shows the importance of calibration to absolute intensity. Therefore, we allowed the core to be swollen by solvent and defined the scattering length density ρ_{core} and the molecular volume of the core as

$$\rho_{core} = \frac{b_{core}}{V_{m,\,core}} = \frac{b_{PA^-} + h b_{solvent} + 0.5 b_{Ca^{2+}}}{V_{m,\,PA^-} + h V_{m,\,solvent} + 0.5 V_{m,\,Ca^{2+}}} \tag{20}$$

with b_{core} being the scattering length and $V_{m,\,core}$ the molecular volume of a monomer in the core. h is the number of solvent molecules per monomer unit. We assumed that every Ca^{2+} binds to two PA^- monomer units. Previous works using isothermal titration calorimetry and calcium selective electrodes [25] suggest that Ca^{2+} binds quantitatively to PA.

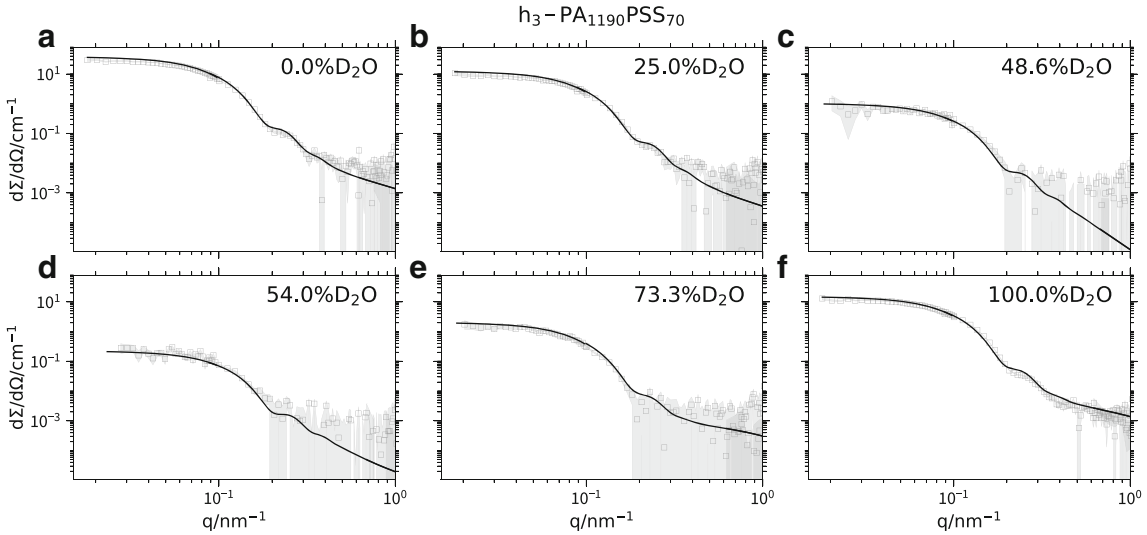

Fig. 7 SANS profiles of h_3-$PA_{1190}PSS_{70}$ micelles (c_{poly} = 4gL^{-1}, $c_{Ca^{2+}}$ = 25 mmol L^{-1}) in 0.0% D_2O (**a**), 25.0% D_2O (**b**), 48.6% D_2O (**c**), 54.0% D_2O (**d**), 73.3% D_2O (**e**), and 100.0% D_2O (**f**). The solid lines represent fits to the form factor of a polydisperse block copolymer micelle [28]. An overview of the fit results can be found in Table 2 and Table S3 of the Supporting Information

The volume fraction of water in the core can be calculated by

$$f_{\text{solvent}} = 1 - \frac{\left(V_{\text{m, PA}^-} + 0.5V_{\text{m, Ca}^{2+}}\right)\text{DP}_{\text{core}}N_{\text{agg}}}{\frac{4}{3}\pi R_{\text{core}}^3} \quad (21)$$

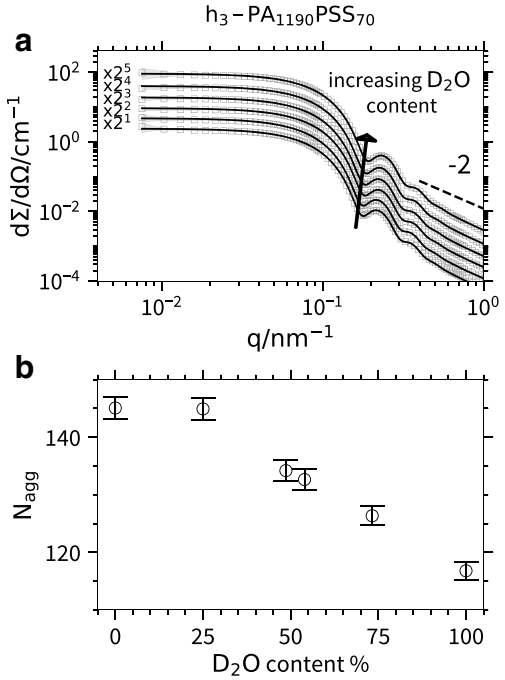

Fig. 8 **a** SAXS profiles of h_3-$PA_{1190}PSS_{70}$ micelles (c_{poly} = 4gL^{-1}, $c_{Ca^{2+}}$ = 25 mmol L^{-1}) in 0.0%, 25.0%, 48.6% , 54.0%, 73.3%, and 100.0% D_2O. The solid lines represent fits to the form factor of a polydisperse block copolymer micelle [28]. An overview of the fit results can be found in Table 2 and Table S3 of the Supporting Information. **b** Aggregation number of the micelles as a function of D_2O content

where DP_{core} is the degree of polymerization of the core block.

The molar volume of condensed Ca^{2+} $V_{\text{m, Ca}^{2+}}$ was left free as a fit parameter since the value based on the ionic radius (2.5 cm^{3}mol^{-1}) [50] and the solvated ion (-28.9 cm^{3}mol^{-1}) [50] did not give satisfactory results. From the fits of the three block copolymer micelles, an averaged value of $V_{m,Ca^{2+}}$ = 17.0± 2.8 cm^{3}mol^{-1} was obtained. Unlike the negative molar volume of the solvated ion, the value we found is positive, which is attributed to the release of hydrated water molecules upon complexation with PA.

From the fits, a quite high volume fraction of 83–85 % water in the core of the micelles is obtained. This corresponds to roughly 12 water molecules per monomer unit. In order to achieve the same core volume without solvent in the core, an aggregation number of 874 would be necessary for d_3-$PA_{360}PSS_{400}$, which can be safely excluded from fitting the data on absolute scale and given polymer concentration. Similar water contents have been observed for the core of Pluronic P123 micelles [51].

The core size results from the aggregation number, degree of polymerization of the PA block, molar volumes of PA, Ca^{2+}, and the water molecules in the core. For d_3-$PA_{360}PSS_{400}$, a rather small core radius of R_{core} = 8.8 nm together with a well-defined standard deviation of 6.9 % for the log-normal distribution was found. In contrast, for d_3-$PA_{1190}PSS_{70}$ and h_3-$PA_{1190}PSS_{70}$, a considerably larger micelle core of 23.7 nm and 22.3 nm was found. This arises from the longer PA block and the higher aggregation numbers of those micelles compared to the polymer with equal ratios of d_3-PA and PSS. The distribution in aggregation numbers and consequently the distribution of the core radius for d_3-$PA_{1190}PSS_{70}$ and h_3-$PA_{1190}PSS_{70}$ is

Table 2 Structural parameters resulting from the analysis of the SANS and SAXS profiles with the form factor of a polydisperse block copolymer micelle [28]. An extended version of the table including error bars can be found in the Supporting Information

	d_3-$PA_{360}PSS_{400}$	d_3-$PA_{1190}PSS_{70}$	h_3-$PA_{1190}PSS_{70}$
N_{agg}	19.1	125.9[a]	116.8[a]
R_{core}/nm	8.8	23.7[a]	22.3[a]
$\frac{\sigma_{R_{core}}}{R_{core}}$	0.069	0.102	0.105
$R_{g,corona}$/nm	8.55	2.12	2.07
s/nm	8.9	4.05	3.53
ν	1.19	0.0	0.0
$f_{solvent}$	0.85	0.85	0.83
$V_{m,Ca^{2+}}/cm^3mol^{-1}$	19.6	17.3	14.0
R_h/nm[b]	26.2 ± 0.9	30.9 ± 1.0	34.0 ± 1.0

[a]Quantity shown for the sample in 100 % D_2O

[b]Hydrodynamic radius obtained from dynamic light scattering

also narrow but slightly broader than that of sample d_3-$PA_{360}PSS_{400}$, resulting in a value of $\frac{\sigma_{R_{core}}}{R_{core}} = 10.2$ % and 10.5 %, respectively. This is in particular visible in the SAXS profiles, which show well-defined oscillations.

The radial scattering length density profiles of the micelles are shown in Fig. 9b–d. The density profile of the PSS corona was assumed to be Gaussian and is determined by the standard deviation s. It was shown previously that the overall dimensions of the corona of block copolymer micelles containing polyelectrolytes cannot safely be determined by small-angle scattering [49], as it is not trivial to define a reasonable cutoff criteria for the scattering length density of the corona. Hence, Förster [49] suggested using the hydrodynamic radius to estimate the dimension of the corona including the part with very low volume fractions on the surface of the micelle. Therefore, the scattering length density profiles shown in Fig. 9b–d also indicate the hydrodynamic dimensions of the micelles measured by dynamic light scattering. Using this approach, the corona covers nearly $2 \cdot R_{g,corona}$, with $R_{g,corona}$ the radius of gyration of the polymer chain in the corona resulting from the Pedersen-Schurtenberger form factor [36]. We conclude that this method is a reasonable approach to estimate the overall dimensions of the corona.

The scattering length density profiles in Fig. 9 show the homogeneous micelle core composed of d_3-PA/h_3-PA, which is complexed by Ca^{2+} and considerably bigger for the h_3-$PA_{1190}PSS_{70}$/ d_3-$PA_{1190}PSS_{70}$ micelles. Vice versa, the profiles highlight the substantially bigger corona for d_3-$PA_{360}PSS_{400}$ compared to h_3-$PA_{1190}PSS_{70}$/d_3-$PA_{1190}PSS_{70}$. The parameter s controlling the thickness of the corona is similar for d_3-$PA_{1190}PSS_{70}$ (4.05 nm) and h_3-$PA_{1190}PSS_{70}$ (3.53 nm), being in agreement with the radius of gyration $R_{g,corona}$ of 2.12 nm (d_3-$PA_{1190}PSS_{70}$) and 2.07 nm (h_3-$PA_{1190}PSS_{70}$).

The relatively small dimensions of the corona for h_3-$PA_{1190}PSS_{70}$/d_3-$PA_{1190}PSS_{70}$ pose the question if it is

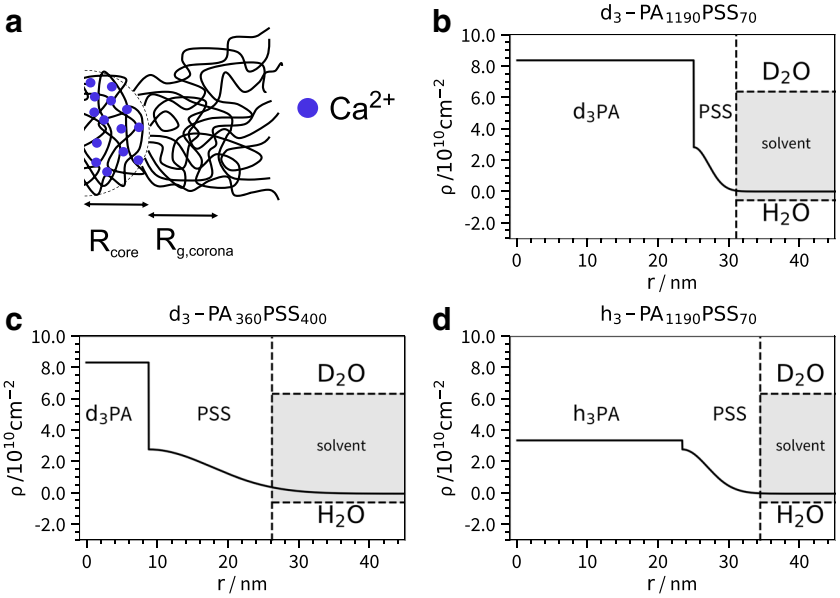

Fig. 9 **a** Sketch of the d_3-$PA_{360}PSS_{400}$ micelles. **b** Scattering length density profile of d_3-$PA_{1190}PSS_{70}$ micelles. **c** Scattering length density profile of d_3-$PA_{360}PSS_{400}$ micelles. **d** Scattering length density profile of h_3-$PA_{1190}PSS_{70}$ micelles. The vertical dashed lines indicate the hydrodynamic dimensions of the micelles. The horizontal dashed lines indicate the scattering length density of H_2O ($-0.558 \cdot 10^{-10}cm^{-2}$) and D_2O ($6.355 \cdot 10^{-10}cm^{-2}$)

necessary to consider the PSS corona in the data analysis. Therefore, SANS curves of two selected contrasts (48.6 % and 100 % D_2O) and a SAXS curve of d_3-$PA_{1190}PSS_{70}$ were analyzed with the model of a polydisperse sphere and are shown in Figure S5 of the Supporting Information. The model describes the contrast, where PSS is matched well (48.6 % D_2O). However, for the SANS curve with the contrast in 100 % D_2O and the SAXS curve, the model fails to describe the high q part as here the corona scattering contributes to the signal.

Besides the corona dimension, the interaction of the polymer chains in the corona can be derived from ν [28]. It has been demonstrated by Monte Carlo simulations that the corona of block copolymer micelles can be treated as quasi-two-dimensional dilute or semi-dilute polymer solution with an osmotic compressibility κ related to ν by $\kappa = 1+\nu$ [35]. Moreover, ν depends on the reduced surface coverage $\frac{\Sigma}{\Sigma^*}$

$$\frac{\Sigma}{\Sigma^*} = \frac{N_{\text{agg}} R_{g,\text{ corona}}^2}{4(R_{\text{core}} + R_{g,\text{corona}})^2} \tag{22}$$

according to a power law [28]. The reduced surface coverage is the two-dimensional analogue of $\frac{c}{c^*}$, where c^* is the overlap concentration [28]. The reduced surface coverage for d_3-$PA_{360}PSS_{400}$ is 1.3, which is above the critical value of unity for the overlap of the chains. This is compatible with the value of $\nu = 1.19$ inferred from the analysis of the scattering profiles. We thus conclude that the PSS chains in the corona of d_3-$PA_{360}PSS_{400}$ micelles are overlapping.

When calculating the reduced surface coverage for h_3-$PA_{1190}PSS_{70}$ and d_3-$PA_{1190}PSS_{70}$, one obtains 0.23 and 0.22, which is significantly smaller than 1.0, indicating that the chains in the corona do not overlap. This is in agreement with the values of ν, which converged to the lower boundary of 0.0 for both samples. The coronas of d_3-$PA_{1190}PSS_{70}$ and h_3-$PA_{1190}PSS_{70}$ micelles contain PSS chains which are not interacting and do not overlap. To confirm this hypothesis, we also analyzed the scattering profiles with a block copolymer form factor, assuming Gaussian chains grafted to the surface of a hard sphere [52]. This form factor is less general than the one used before since it is only valid for low surface coverage. The details of the model can be found in the Supporting Information (Figures S1-S3). We were able to describe the scattering data of d_3-$PA_{1190}PSS_{70}$ and h_3-$PA_{1190}PSS_{70}$ micelles with similar fit quality and micelle dimensions. However, when the simpler model [52] was applied to the profiles of d_3-$PA_{360}PSS_{400}$, we were not able to fit the contrast shown in Fig. 3d–f satisfactorily. The best fit with this model is also shown in Figure S3 of the Supporting Information. The simpler model [52] does not allow to take into account interactions between the chains in the corona by a ν parameter and thus fails to reproduce the scattering signal which is dominated by the corona. Accordingly, the polymer chains in the corona for d_3-$PA_{1190}PSS_{70}$/h_3-$PA_{1190}PSS_{70}$ micelles are not overlapping, whereas PSS chains in d_3-$PA_{360}PSS_{400}$ micelles are overlapping.

We conclude the section by stressing again that the H_2O/D_2O ratio influences the aggregation number of d_3-$PA_{1190}PSS_{70}$/h_3-$PA_{1190}PSS_{70}$. This effect deserves further consideration. Figures 6b and 7b show that the obtained aggregation numbers of the micelles decrease with increasing content of heavy water. This slight decrease in aggregate size is attributed to an isotope effect occurring upon change of the solvent from light to heavy water, irrespective of the use of deuterated or hydrogenated PA and will be addressed in detail in the next section.

Isotope effect

In the previous section, it was found that the size of d_3-$PA_{1190}PSS_{70}$ and h_3-$PA_{1190}PSS_{70}$ micelles slightly decreases with increasing D_2O content. For the form factor fits, this changing micelle size was taken into account by attributing an individual aggregation number to each contrast and using this N_{agg} for the corresponding SANS and SAXS curves at the respective contrast.

This change in aggregation number is caused by an isotope effect occurring upon change of the solvent from light to heavy water and is observed for a polymer with a deuterated PA block as well as a hydrogenated PA block. Preceding works have shown that the solvent quality and the phase behavior of polymer-solvent systems can change if hydrogenated solvents are replaced by deuterated solvents [53]. Moreover, it has been shown that the phase boundaries of proteins in the presence of multivalent cations may change when going from light to heavy water [54]. These effects arise from the slightly different interaction of the deuterated solvent with the macromolecule. This seems to be also the case for the present system.

The isotope effect only appears for d_3-$PA_{1190}PSS_{70}$ and h_3-$PA_{1190}PSS_{70}$ but not for d_3-$PA_{360}PSS_{400}$. As the effect only appears for the polymers with the long PA block, it is possible that the binding of Ca^{2+} to PA plays an important role in the process. In order to clarify if the isotope effect is accompanied by a difference in binding of Ca^{2+} to PA in H_2O or D_2O isothermal titration calorimetry was performed in light and heavy water. This technique measures the heat of binding upon addition of Ca^{2+} to a solution of PA. Figure 10 shows the titration curves in H_2O and D_2O as well as the fit to the model of a single set of identical binding sites [46, 47]. Table 3 summarizes the obtained enthalpy of binding ΔH°, entropy of binding $T\Delta S^{\circ}$, binding constant K, and stochiometry of binding n. From the titration curves, it is clear that the binding in H_2O and D_2O have identical

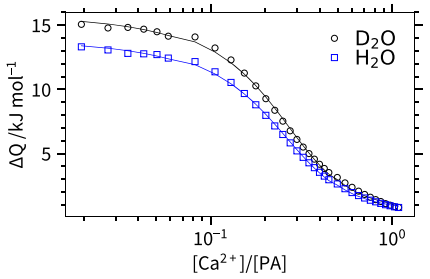

Fig. 10 Isothermal titration curves of PA homopolymer in the presence of Ca^{2+} in H_2O and D_2O. The curve shows the heat of binding per injection as a function of Ca^{2+}/PA ratio. The solid lines are fits with the model of a single set of identical binding sites. Table 3 summarizes the results of the data analysis

binding constants K; however, the enthalpy of binding $\Delta H^{\ominus}$ and the entropy of binding $T\Delta S^{\ominus}$ is slightly larger for the titration in D_2O. We attribute this slight difference also to an isotope effect and conclude that this isotope effect controls the binding of Ca^{2+} and the aggregation number of the micelles.

Stuhrmann analysis

In Section 2, it was shown that the SANS profiles from the contrast variation experiment can be well described by a suitable form factor model [28]. However, such an analytical expression for a form factor model is not always available, in particular for systems which are not as well-defined as block copolymer micelles. Moreover, deuteration is not always feasible as deuterated monomers do not exist for a wide range of polymers and deuteration of biological molecules such as proteins or sugars is often difficult and very cost intensive. Nevertheless, a contrast variation experiment is still possible if the scattering length densities of two components are sufficiently different.

In order to be able to analyze contrast variation experiments, Stuhrmann [29, 30] developed a model-indepedent approach, the so called Stuhrmann analysis. In the present section, this approach is employed for d_3-$PA_{1190}PSS_{70}$ as well as d_3-$PA_{360}PSS_{400}$ and compared with the results from the form factor fits. Eventually, the potential of the method is demonstrated by applying it to the data of h_3-$PA_{1190}PSS_{70}$, nicely demonstrating that reliable structural information can be obtained even from a fully hydrogenated polymer and more importantly without necessarily using form factor fits.

Figure 11a shows the square root of the coherent SANS scattering intensity at $q \rightarrow 0$ for the measured contrasts as a function of D_2O content for all three samples. We used N_{agg} (determined from the form factor fits) for the samples d_3-$PA_{1190}PSS_{70}$ and h_3-$PA_{1190}PSS_{70}$ to normalize the coherent forward intensity from SANS in order to account for the effect of a change in aggregation number. The data follow a linear behavior as first shown by Stuhrmann [29, 30] which is expected when the contrast term $\Delta\rho$ is changed. A linear fit of the data shows that the match points of the block copolymer micelles is at 64.3 ± 0.4 % D_2O (d_3-$PA_{360}PSS_{400}$), 125.6 ± 0.7 % D_2O (d_3-$PA_{1190}PSS_{70}$), and 57.4±0.6 % D_2O (h_3-$PA_{1190}PSS_{70}$). Based on the chemical composition of the block copolymer and the scattering length densities of the two blocks, the theoretical match point of the block copolymers and their micelles can be calculated. The theoretical matchpoint for all three polymers is close to the experimentally found, which confirms the successful synthesis and preliminary characterization of the block copolymer.

Table 3 Results of the ITC experiments probing the binding of Ca^{2+} to PA in H_2O and D_2O at 25 °C

	H_2O	D_2O
K/L mol^{-1}	$6.3 \cdot 10^3 \pm 0.3 \cdot 10^3$	$6.4 \cdot 10^3 \pm 0.5 \cdot 10^3$
$\Delta H^{\ominus}$/kJ mol^{-1}	17.45 ± 0.34	19.76 ± 0.56
$T\Delta S^{\ominus}$/kJ mol^{-1}	39.14 ± 0.46	41.49 ± 0.75
$\Delta G^{\ominus}$/kJ mol^{-1}	−21.69 ± 0.12	−21.73 ± 0.19
n	0.231 ± 0.002	0.239 ± 0.003

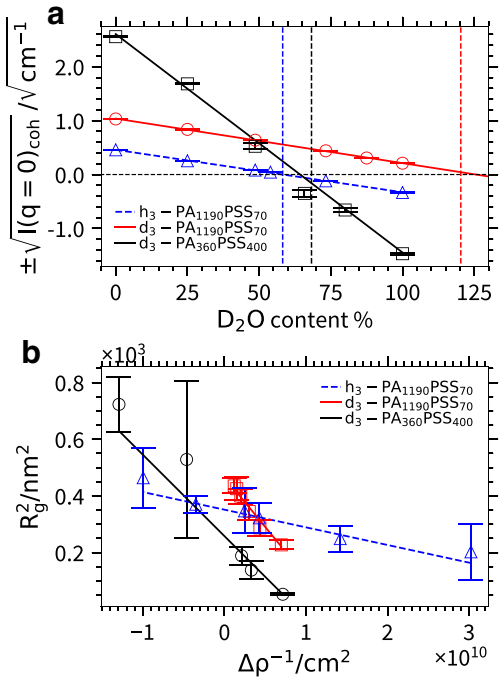

Fig. 11 **a** Coherent forward scattering for d_3-$PA_{360}PSS_{400}$, d_3-$PA_{1190}PSS_{70}$, and h_3-$PA_{1190}PSS_{70}$ from SANS as a function of D_2O content. The solid line represents a linear fit to the data. The data for d_3-$PA_{1190}PSS_{70}$ and h_3-$PA_{1190}PSS_{70}$ are normalized by the aggregation number N_{agg}. The vertical dashed lines indicate the theoretical match points calculated from the chemical composition. **b** Squared radius of gyration R_g^2 as a function of inverse scattering contrast for d_3-$PA_{360}PSS_{400}$, d_3-$PA_{1190}PSS_{70}$ and h_3-$PA_{1190}PSS_{70}$. The straight lines are fit to Eq. 23 [29, 30]

Further, more quantitative information can be extracted from the scattering curves by plotting the squared apparent radius of gyration R_g^2 from a Guinier analysis at low q as a function of the inverse scattering contrast $\Delta\rho^{-1}$. Figure 11 b shows the so called Stuhrmann plot [29, 30]. Ibel and Stuhrmann [29, 30] showed that for a two-component system R_g^2 depends on $\Delta\rho^{-1}$ as

$$R_g^2 = R_m^2 + \alpha\Delta\rho^{-1} + \gamma\Delta\rho^{-2} \tag{23}$$

with R_m being the radius of gyration at infinite contrast. The coefficient α is related to the second moment of the scattering length density fluctuations about its mean value. The coefficient γ is the square of the first moment of the density fluctuations about the mean. If α is positive, the component of the lower scattering length density is located more towards the inside of the objects. For a negative value of α, the component with the higher scattering length density is concentrated in the inside. γ is proportional to the squared separation of the two components, with $\gamma = 0$ indicating that the centers-of-mass are coinciding.

Figure 11 b shows R_g^2 as a function of $\Delta\rho^{-1}$ for the three samples. For all three polymers, the points follow a straight line with γ being close to zero and with a negative slope α.

For all three samples, a negative value for α indicates that the PA blocks are always located in the core of the micelles. It may not have been clear at the outset of the experiment that this also holds for the fully hydrogenated sample h_3-$PA_{1190}PSS_{70}$. However, calculation of the scattering length densities ρ for PSS ($2.82 \cdot 10^{10}\text{cm}^{-2}$) and h_3-PA ($4.21 \cdot 10^{10}\text{cm}^{-2}$) reveals that they are sufficiently different also for the fully hydrogenated sample, with h_3-PA having a larger ρ. This nicely demonstrates the benefit of additionally analyzing a fully hydrogenated sample.

The fact that γ is close to zero shows that the center-of-mass of PSS and d_3-PA/h_3-PA coincide. Such a situation is only compatible with a highly symmetrical core-shell structure of the micelles. Furthermore, the scattering curves do not show any indication for the presence of cylindrical or vesicular micelles, which would also be compatible with a value of γ close to zero. Accordingly, we can already conclude from the model free analysis and without using information from the form factor fits that the micelles are spherical with a core composed of d_3-PA/h_3-PA and a corona of PSS, being in full agreement with the form factor fits.

Using the parallel axis theorem, one can relate α and R_m^2 to the radius of gyration of the core $R_{g,\text{core}}$ and the radius of gyration of the shell $R_{g,\text{shell}}$ [55]

$$R_m^2 = f_{\text{core}} R_{g,\text{core}}^2 + f_{\text{shell}} R_{g,\text{shell}}^2 \tag{24}$$

$$\alpha = (\rho_{\text{core}} - \rho_{\text{shell}}) f_{\text{core}} f_{\text{shell}} (R_{g,\text{core}}^2 - R_{g,\text{shell}}^2) \tag{25}$$

with f_{core} and f_{corona} being the volume fraction of core and corona block and ρ_{core} and ρ_{corona} the scattering length densities of the core and corona block, respectively. All the information is available from the chemical composition and molar volumes of the monomer units. Equations 24 and 25 can be solved for $R_{g,\text{core}}$ and $R_{g,\text{shell}}$, making the dimensions of the micelles directly accessible from a model-independent analysis of the scattering data. Table 4 summarizes the values of R_m, α, $R_{g,\text{core}}$, and $R_{g,\text{shell}}$ for all three samples.

For d_3-$PA_{360}PSS_{400}$, a value of $R_{g,\text{core}} = 7.1$ nm and $R_{g,\text{shell}} = 18.0$ nm is found. This indicates that the micelles contain a d_3-PA core which is surrounded by a rather thick shell of PSS, in perfect agreement with the scattering length density profiles obtained from the form factor fits. The core radius R_{core} from the form factor fits can be used to calculate a value for $R_{g,\text{core}}$ by [31]

$$R_{g,\text{ core}} = \sqrt{\frac{3}{5}} R_{\text{core}} \tag{26}$$

$R_{g,\text{core}}$ calculated accordingly is 6.8 nm, in perfect agreement with the value obtained from the model independent analysis (7.1 ± 2.5 nm).

Using Eqs. 24–25 for d_3-$PA_{1190}PSS_{70}$ yields $R_{g,\text{core}} = 19.9$ nm and $R_{g,\text{shell}} = 29.7$ nm, nicely illustrating the considerably bigger d_3-PA core for this sample and the rather thin PSS corona. Comparing the core radius from the form factor analysis with $R_{g,\text{core}}$ using Eq. 26 yields a value of 18.4 nm from the form factor fit. This shows a good agreement between both methods, in particular when taking into account that the isotope effect and therefore the slightly changing micelle dimensions is not considered in Fig. 11b of the Stuhrmann analysis.

Finally, the micelle dimensions for the fully hydrogenated polymer h_3-$PA_{1190}PSS_{70}$ are calculated. The values of $R_{g,\text{core}} = 16.8$ nm and $R_{g,\text{shell}} = 30.1$ nm are very similar to the results found for d_3-$PA_{1190}PSS_{70}$ micelles, showing that the h_3-$PA_{1190}PSS_{70}$ micelles also consist of a

Table 4 Micelle dimensions obtained from the Stuhrmann plot (R_g^2 versus $\Delta\rho^{-1}$)

Polymer	R_m/ nm	α	$R_{g,\text{core}}$/ nm	$R_{g,\text{shell}}$/ nm
d_3-$PA_{360}PSS_{400}$	16.1 ± 1.4	$(-2.9 \pm 0.3)10^6$	7.1 ± 2.5	18.0 ± 1.7
d_3-$PA_{1190}PSS_{70}$	21.6 ± 1.0	$(-3.5 \pm 0.4)10^6$	19.9 ± 1.1	29.7 ± 4.9
h_3-$PA_{1190}PSS_{70}$	18.7 ± 1.2	$(-6.2 \pm 2.5)10^5$	16.8 ± 2.3	30.1 ± 5.1

large PA core and a thin PSS corona. The radius of gyration of the core according to Eq. 26 and the form factor fit is 17.3 nm, which is in perfect agreement with the result from the Stuhrmann plot (16.8 ± 2.3 nm).

The quantitative discussion presented above is a nice verification of the power of the Stuhrmann analysis, for which we could provide a highly suitable model system. The model-independent analysis does not only offer values for important size parameters of the micelles, but provides evidence for a core-shell structure of these micelles, with the PA blocks located at the core of the micelles. These features and conclusions could be consistently and independently derived from investigating three different block copolyelectrolyte samples of the type PA-*b*-PSS. This nicely shows the potential of the model free analysis given in the present section and at the same time confirms the form factor fits.

Conclusion

We investigated self-assemblies of block copolymers of the two polyelectrolytes polyacrylate (PA) and polystyrene sulfonate (PSS) by a combination of contrast variation small-angle neutron scattering, small-angle X-ray scattering, and dynamic light scattering. In a previous work [27], we showed that such block copolymers form well-defined micelles in the presence of Ca^{2+}. In order to investigate the morphology of these micelles, the PA block was selectively deuterated.

First and foremost, SANS and SAXS reveal a spherical micellar shape for the aggregates with a well-defined size and a low polydispersity for three different block copolyelectrolytes of the type PA-*b*-PSS, using the model of a block copolymer micelle with a homogeneous scattering length density in the core and self-avoiding chains in the corona [28]. Model interpretation confirmed the micellar shape of the aggregates and unambiguously proved that Ca^{2+} cations are binding to PA and that this complex forms the hydrophobic core of the micelles. This core contains up to 85 vol% of water. PSS forms the corona of the micelles and adopts the conformation of self-avoiding polymer chains. Furthermore, we found that the PSS chains in the corona do not overlap for a block copolymer with a high fraction of PA, while they start to show excluded volume effects once they overlap due to an increase of the PSS fraction. As the interactions of the Ca^{2+} cations with the PSS chains are only non-specific being dominated by electrostatically based screening of electrostatic forces, the resulting PSS corona stabilizes the micelles and keeps the phase separation otherwise observed with pure PA and Ca^{2+} confined to the core of the micelles.

For a set of block copolymers with a long PA and a short PSS block, a small change in dimensions was observed in the SAXS profiles when going from H_2O to D_2O. This was attributed to an isotope effect arising from a slightly different binding enthalpy of Ca^{2+} to PA in H_2O and D_2O. Having SAXS and contrast variation SANS data available, it was possible to take this into account in the data analysis as a change in aggregation number. Such effects are at risk to be neglected in SANS based contrast variation experiments and the present example stresses the importance of combining SAXS and SANS in order to elucidate such effects and take them into account during the data analysis.

Finally, we demonstrated that contrast variation can also be performed on a fully hydrogenated block copolymer as long as the scattering length densities of the blocks are sufficiently different. In combination with the SAXS data, it was possible to reliably determine the size, structure, and morphology of the micelles. This is particularly interesting for samples where deuteration is not possible and nicely illustrates the future potential of novel, more powerful neutron sources.

Acknowledgements The authors thank the Institut Laue-Langevin (https://doi.ill.fr/10.5291/ILL-DATA.9-11-1888) and the European Synchrotron Radiation Facility for the provision of beam time, the Partnership for Soft Condensed Matter (PSCM) for supply of the light scattering, and Narayanan Theyencheri and the ID02 team for the supply of in-house time at ID02. N.C. acknowledges funding for a PhD scholarship from Institut Laue-Langevin.

Funding Information Open Access funding provided by Projekt DEAL.

Compliance with Ethical Standards

Conflict of interests The authors declare that they have no conflict of interest.

Dedication The authors are happy to dedicate this work on small-angle scattering of block copolyelectrolytes to Matthias Ballauff. The block copolyelectrolytes reversibly form micelles in response to interactions with Ca^{2+} cations. It is a happy coincidence that this work nicely fits into the broader scope of Matthias' scientific work. This does not come as a surprise though as Matthias' accomplishments inspired the present as well as some of our other work. Above all, the authors are grateful to him for having introduced them to the power of ASAXS. They wish Matthias Ballauff all the best for his future!

References

1. Volk N, Vollmer D, Schmidt M, Oppermann W, Huber K (2004) Conformation and phase diagrams of flexible polyelectrolytes 166:29–65. https://doi.org/10.1007/b11348
2. Chiappisi L, Hoffmann I, Gradzielski M (2013) Complexes of oppositely charged polyelectrolytes and surfactants – recent developments in the field of biologically derived polyelectrolytes. Soft Matter 9(15):3896. https://doi.org/10.1039/c3sm27698h. http://pubs.rsc.org/en/content/articlehtml/2013/sm/c3sm27698h
3. Bain CD, Claesson PM, Langevin D, Meszaros R, Nylander T, Stubenrauch C, Titmuss S, von Klitzing R (2010) Complexes of surfactants with oppositely charged polymers at surfaces and in bulk. Adv Colloid Interface Sci 155(1-2):32–49. https://doi.org/10.1016/j.cis.2010.01.007
4. Tummino A, Toscano J, Sebastiani F, Noskov BA, Varga I, Campbell RA (2018) Effects of aggregate charge and subphase ionic strength on the properties of spread polyelectrolyte/surfactant films at the air/water interface under static and dynamic conditions. Langmuir p acs.langmuir.7b03960 https://doi.org/10.1021/acs.langmuir.7b03960
5. Szilagyi I, Trefalt G, Tiraferri A, Maroni P, Borkovec M (2014) Polyelectrolyte adsorption, interparticle forces, and colloidal aggregation. Soft Matter 10(15):2479–2502. https://doi.org/10.1039/c3sm52132j
6. Bolto B, Gregory J (2007) Organic polyelectrolytes in water treatment. Water Res 41(11):2301–2324. https://doi.org/10.1016/j.watres.2007.03.012
7. Pochard I, Labbez C, Nonat A, Vija H, Jönsson B (2010) The effect of polycations on early cement paste. Cem Concr Res 40 (10):1488–1494. https://doi.org/10.1016/j.cemconres.2010.06.002
8. Marchon D, Sulser U, Eberhardt A, Flatt RJ (2013) Molecular design of comb-shaped polycarboxylate dispersants for environmentally friendly concrete. Soft Matter 9(45):10719–10728. https://doi.org/10.1039/c3sm51030a
9. Llamas S, Guzmán E, Ortega F, Baghdadli N, Cazeneuve C, Rubio RG, Luengo GS (2015) Adsorption of polyelectrolytes and polyelectrolytes-surfactant mixtures at surfaces: a physicochemical approach to a cosmetic challenge. Adv Colloid Interface Sci 222:461–487. https://doi.org/10.1016/j.cis.2014.05.007
10. Huber K (1993) Calcium-induced shrinking of polyacrylate chains in aqueous solution. J Phys Chem 97(38):9825–9830. https://doi.org/10.1021/j100140a046
11. Michaeli I (1960) Ion binding and the formation of insoluble polymethacrylic salts. J Polym Sci Xlviii XLVIII:291–299
12. Goerigk G, Schweins R, Huber K, Ballauff M (2004) The distribution of Sr2+ counterions around polyacrylate chains analyzed by anomalous small-angle X-ray scattering. Europhys Lett 66(3):331–337. https://doi.org/10.1209/epl/i2003-10215-y. http://stacks.iop.org/0295-5075/66/i=3/a=331?key=crossref.88d02ca60a935e4a08a53581a63526b2
13. Schweins R, Goerigk G, Huber K (2006) Shrinking of anionic polyacrylate coils induced by Ca2+, Sr2+ and Ba2+: a combined light scattering and ASAXS study. Eur Phys J E 21(2):99–110. https://doi.org/10.1140/epje/i2006-10047-7
14. Goerigk G, Huber K, Schweins R (2007) Probing the extent of the Sr2+ ion condensation to anionic polyacrylate coils: a quantitative anomalous small-angle x-ray scattering study. J Chem Phys 127(15):154908. https://doi.org/10.1063/1.2787008
15. Lages S, Goerigk G, Huber K (2013) SAXS And ASAXS on dilute sodium polyacrylate chains decorated with lead ions. Macromolecules 46(9):3570–3580. https://doi.org/10.1021/ma400427d
16. Hansch M, Hämisch B, Schweins R, Prévost S, Huber K (2018) Liquid-liquid phase separation in dilute solutions of poly(styrene sulfonate) with multivalent cations: phase diagrams, chain morphology, and impact of temperature. J Chem Phys 148(1):014901. https://doi.org/10.1063/1.5006618
17. Narh KA, Keller A (1993) Precipitation effects in polyelectrolytes on addition of salts. J Polym Sci Part B Polym Phys 31(2):231–234. https://doi.org/10.1002/polb.1993.090310213
18. Drifford M, Delsanti M (2001) Polyelectrolyte solutions with multivalent added salts: stability, structure, and dynamics. In: Phys. Chem. Polyelectrolytes, CRC Press, pp 157–184
19. de la Cruz MO, Belloni L, Delsanti M, Dalbiez JP, Spalla O, Drifford M (1995) Precipitation of highly charged polyelectrolyte solutions in the presence of multivalent salts. J Chem Phys 103(13):5781–5791. https://doi.org/10.1063/1.470459
20. Hansch M, Kaub HP, Deck S, Carl N, Huber K (2018) Reaction enthalpy from the binding of multivalent cations to anionic polyelectrolytes in dilute solutions. J Chem Phys 148(11):114906. https://doi.org/10.1063/1.5019877
21. Ikeda Y, Beer M, Schmidt M, Huber K (1998) Ca 2+ and cu 2+ induced conformational changes of sodium polymethacrylate in dilute aqueous solution. Macromolecules 31(3):728–733. https://doi.org/10.1021/ma970540p
22. Lages S, Schweins R, Huber K (2007) Temperature-Induced Collapse of alkaline earth Cation-Polyacrylate anion complexes. J Phys Chem B 111(35):10431–10437. https://doi.org/10.1021/jp068258k
23. Schweins R, Huber K (2001) Collapse of sodium polyacrylate chains in calcium salt solutions. Eur Phys J E 5(1):117–126. https://doi.org/10.1007/s101890170093
24. Schweins R, Lindner P, Huber K (2003) Calcium induced shrinking of naPA Chains: a sans investigation of single chain behavior. Macromolecules 36(25):9564–9573. https://doi.org/10.1021/ma0347722
25. Sinn CG, Dimova R, Antonietti M (2004) Isothermal titration calorimetry of the Polyelectrolyte/Water interaction and binding of ca 2+ : effects determining the quality of polymeric scale inhibitors. Macromolecules 37(9):3444–3450. https://doi.org/10.1021/ma030550s
26. Ishiwari F, Hasebe H, Matsumura S, Hajjaj F, Horii-Hayashi N, Nishi M, Someya T, Fukushima T (2016) Bioinspired design of a polymer gel sensor for the realization of extracellular Ca2+ imaging. Sci Rep 6(1):24275. https://doi.org/10.1038/srep24275. http://www.nature.com/articles/srep24275
27. Carl N, Prévost S, Schweins R, Huber K (2019) Ion-selective binding as a new trigger for micellization of block copolyelectrolytes with two anionic blocks. Soft Matter. https://doi.org/10.1039/C9SM01138B
28. Svaneborg C, Pedersen JS (2002) Form factors of block copolymer micelles with excluded-volume interactions of the corona chains determined by monte carlo simulations. Macromolecules 35(3):1028–1037. https://doi.org/10.1021/ma011046v
29. Stuhrmann HB (1974) Neutron small-angle scattering of biological macromolecules in solution. J Appl Crystallogr 7(2): 173–178. https://doi.org/10.1107/S0021889874009071. http://scripts.iucr.org/cgi-bin/paper?S0021889874009071
30. Ibel K, Stuhrmann H (1975) Comparison of neutron and X-ray scattering of dilute myoglobin solutions. J Mol Biol 93(2):255–265. https://doi.org/10.1016/0022-2836(75)90131-X. https://linkinghub.elsevier.com/retrieve/pii/002228367590131X
31. Zemb T, Lindner P (2002) Neutrons, X-rays and light: scattering methods applied to soft condensed matter. North-Holland

32. Orthaber D, Bergmann A, Glatter O (2000) SAXS Experiments on absolute scale with Kratky systems using water as a secondary standard. J Appl Crystallogr 33(2):218–225. https://doi.org/10.1107/S0021889899015216
33. Boesecke P (2007) Reduction of two-dimensional small- and wide-angle X-ray scattering data. J Appl Crystallogr 40(SUPPL. 1):423–427. https://doi.org/10.1107/S0021889807001100
34. Rayleigh L (1911) Form factor of a homogenous sphere. Proc Roy Soc London A84:25–38
35. Svaneborg C, Pedersen JS (2001) Block copolymer micelle coronas as quasi-two-dimensional dilute or semidilute polymer solutions. Phys Rev E 64(1):010802. https://doi.org/10.1103/PhysRevE.64.010802
36. Skov J, Schurtenberger P, Pedersen JS (1996) Scattering functions of semiflexible polymers with and without excluded volume effects excluded volume effects. Macromolecules 9297(96):7602–7612. https://doi.org/10.1021/ma9607630
37. Chen WR, Butler PD, Magid LJ (2006) Incorporating intermicellar interactions in the fitting of SANS data from cationic wormlike micelles. Langmuir 22(15):6539–6548. https://doi.org/10.1021/la0530440
38. Sommer C, Pedersen JS, Garamus VM (2005) Structure and interactions of block copolymer micelles of brij 700 studied by combining small-angle X-ray and neutron scattering. Langmuir 21(6):2137–2149. https://doi.org/10.1021/la047489k
39. Pedersen JS, Posselt D, Mortensen K (1990) Analytical treatment of the resolution function for small-angle scattering. J Appl Crystallogr 23(4):321–333. https://doi.org/10.1107/S0021889890003946. http://scripts.iucr.org/cgi-bin/paper?S0021889890003946
40. Muthig M, Prévost S, Orglmeister R, Gradzielski M (2013) SASET: a program for series analysis of small-angle scattering data. J Appl Crystallogr 46(4):1187–1195. https://doi.org/10.1107/S0021889813016658
41. Frisken BJ (2001) Revisiting the method of cumulants for the analysis of dynamic light-scattering data. Appl Opt 40(24):4087. https://doi.org/10.1364/AO.40.004087. https://www.osapublishing.org/abstract.cfm?URI=ao-40-24-4087
42. Burchard W, Schmidt M, Stockmayer WH (1980) Influence of hydrodynamic preaveraging on Quasi-Elastic scattering from flexible linear and Star-Branched macromolecules. Macromolecules 13(3):580–587. https://doi.org/10.1021/ma60075a020
43. Burchard W, Schmidt M, Stockmayer WH (1980) Information on polydispersity and branching from combined Quasi-Elastic and intergrated scattering. Macromolecules 13(5):1265–1272. https://doi.org/10.1021/ma60077a045
44. Cho CH, Urquidi J, Singh S, Robinson GW (1999) Thermal offset viscosities of liquid h 2O, d 2O, and t 2O. J Phys Chem B 103(11):1991–1994. https://doi.org/10.1021/jp9842953
45. Scheuermann TH, Brautigam CA (2015) High-precision, automated integration of multiple isothermal titration calorimetric thermograms: New features of NITPIC. Methods 76:87–98. https://doi.org/10.1016/j.ymeth.2014.11.024
46. Wiesman T, Williston S, Brandts JF (1989) Rapid measurement of binding constants and heats of binding using ITC. Anal Biochem 179:131–137. https://doi.org/10.1016/0003-2697(89)90213-3
47. Merabet E, Ackers GK (1995) Calorimetric analysis of λ cI repressor binding to DNA operator sites. Biochemistry 34(27):8554–8563. https://doi.org/10.1021/bi00027a005
48. Tondre C, Zana R (1972) Apparent molal volumes of polyelectrolytes in aqueous solutions. J Phys Chem 76(23):3451–3459. https://doi.org/10.1021/j100667a026
49. Förster S, Hermsdorf N, Böttcher C, Lindner P (2002) Structure of polyelectrolyte block copolymer micelles. Macromolecules 35(10):4096–4105. https://doi.org/10.1021/ma011565y
50. Marcus Y (1997) Ion Properties Marcel Dekker. New York, New York
51. Manet S, Lecchi A, Impéror-Clerc M, Zholobenko V, Durand D, Oliveira CLP, Pedersen JS, Grillo I, Meneau F, Rochas C (2011) Structure of Micelles of a Nonionic Block Copolymer Determined by SANS and SAXS. J Phys Chem B 115(39):11318–11329. https://doi.org/10.1021/jp200212g
52. Pedersen JS, Gerstenberg MC (1996) Scattering form factor of block copolymer micelles. Macromolecules 29(4):1363–1365. https://doi.org/10.1021/ma9512115
53. Strazielle C, Benoit H (1975) Some thermodynamic properties of Polymer-Solvent systems. Comparison between deuterated and undeuterated systems. Macromolecules 8(2):203–205. https://doi.org/10.1021/ma60044a021
54. Braun MK, Wolf M, Matsarskaia O, Da Vela S, Roosen-Runge F, Sztucki M, Roth R, Zhang F, Schreiber F (2017) Strong isotope effects on effective interactions and phase behavior in protein solutions in the presence of multivalent ions. J Phys Chem B 121(7):1731–1739. https://doi.org/10.1021/acs.jpcb.6b12814
55. Moore PB (1982) 8. Small-Angle Scattering Techniques for the Study of Biological Macromolecules and Macromolecular Aggregates. In: Methods Exp Phys, vol 20. Elsevier, pp 337–390

Nico Carl studied Chemistry (B.Sc.) and Polymer Science (M.Sc.) at the University of Bayreuth. During his master studies, he spent three months at the European Synchrotron Radiation Facility working with Dr. Sylvain Prévost on studying the aggregation of gold nanoparticles with time-resolved X-ray scattering. Since 2016, he has a shared Ph.D. position between the University of Paderborn and the Institut Max von Laue — Paul Langevin under the supervision of Dr. Ralf Schweins and Professor Klaus Huber. His research interest is the self-assembly of polyelectrolytes and the manipulation of self-assembled structures with external stimuli such as light or temperature.

Sylvain Prévost studied Physical Chemistry at the École Nationale Supérieure de Chimie et Physique de Bordeaux (ENSCPB) and obtained in 2006 a Ph.D. in Chemistry and Materials Sciences from the University of Versailles — Saint-Quentin-en-Yvelines under the supervision of Prof. Ch. Larpent and Dr. F. Testard, working in the LIONS at CEA in Saclay in the group of Prof. Th. Zemb and later Prof. J. Daillant. After his Ph.D., he joined the group of Prof. M. Gradzielski at the Technical University of Berlin while working on the Small-Angle Neutron Scattering V4 at Helmzoltz-Zentrum-Berlin, which became part of the Soft Matter and Functional Materials department headed by Prof. M. Ballauff. In 2014, he then came to Grenoble to join Dr. Th. Narayanan on ID02, the high flux SAXS, WAXS, USAXS, ASAXS, and XPCS beam line from ESRF—The European Synchrotron. In 2017, he finally joined Dr. R. Schweins on D11, the long pinhole SANS from the European Neutron Source at the Institut Max von Laue—Paul Langevin (ILL).

Ralf Schweins studied Chemistry at the University of Paderborn from 1993 until 1998. He did his Ph.D. thesis in Physical Chemistry under the supervision of Prof. Klaus Huber. After completing his Ph.D. in 2002, he joined the Institut Laue – Langevin as co-responsible of the Small-Angle Neutron Scattering Instrument D11. In 2007, he became promoted staff scientist and in 2015 first instrument responsible. He is also involved in the Partnership for Soft Condensed Matter between the Institut Laue – Langevin and the European Synchrotron Radiation Facility. His research interests cover polyelectrolytes, colloids, and supramolecular self-assembly of various building blocks.

Klaus Huber studied Chemistry at the University of Freiburg and obtained a Ph.D. in Macromolecular Chemistry from the University of Freiburg under the supervision of Professor W. Burchard. After his Ph.D., he worked with Professor W. H. Stockmayer at Dartmouth College in Hannover, USA, as a Feodor-Lynen Fellow. He then joined Ciba-Geigy in Basel, Switzerland, for nine years as a research and development chemist in the field of Colloid and Interface Science. In 1997, he accepted a position as a professor of Physical Chemistry at the University of Paderborn. His research focuses on morphological changes in soft matter systems including polyelectrolyte solutions, nucleation and growth processes and self-assembly of proteins and dyestuffs.